

# WaRA: Wavelet Low-Rank Adaptation

Moein Heidari<sup>1</sup>, Yijin Huang<sup>1,2</sup>, Yasamin Medghalchi<sup>1</sup>, Alireza Rafiee<sup>3</sup>, Roger Tam<sup>1</sup>, and Ilker Hacihaliloglu<sup>4,5</sup>

<sup>1</sup> School of Biomedical Engineering, The University of British Columbia, Vancouver, BC, Canada

<sup>2</sup> Department of Electronic and Electrical Engineering, Southern University of Science and Technology, Shenzhen, China

<sup>3</sup> Department of Electrical and Computer Engineering, The University of British Columbia, Vancouver, BC, Canada

<sup>4</sup> Department of Radiology, The University of British Columbia, Vancouver, BC, Canada

<sup>5</sup> Department of Medicine, The University of British Columbia, Vancouver, BC, Canada

moein.heidari@ubc.ca

**Abstract.** Adapting large pretrained vision models to medical image classification is often limited by memory, computation, and task-specific specializations. Parameter-efficient fine-tuning (PEFT) methods like LoRA reduce this cost by learning low-rank updates, but operating directly in feature space can struggle to capture the localized, multi-scale features common in medical imaging. We propose WaRA, a wavelet-structured adaptation module that performs low-rank adaptation in a wavelet domain. WaRA reshapes patch tokens into a spatial grid, applies a fixed discrete wavelet transform, updates subband coefficients using a shared low-rank adapter, and reconstructs the additive update through an inverse wavelet transform. This design provides a compact trainable interface while biasing the update toward both coarse structure and fine detail. For extremely low-resource settings, we introduce Tiny-WaRA, which further reduces trainable parameters by learning only a small set of coefficients in a fixed basis derived from the pretrained weights through a truncated SVD. Experiments on medical image classification across four modalities and datasets demonstrate that WaRA consistently improves performance over strong PEFT baselines, while retaining a favorable efficiency profile. Our code is publicly available at [GitHub](#).

**Keywords:** Parameter-efficient fine-tuning · Low-rank adaptation · Pre-trained models.

## 1 Introduction

Medical image analysis has substantially advanced through the deep learning era, despite the data-intensive requirements of modern foundation models. Curating large-scale annotated medical datasets remains particularly challenging due to privacy constraints, the severe class imbalances inherent in clinical data, and

the high cost of expert annotation. Transfer learning and Parameter-Efficient Fine-Tuning (PEFT) have therefore become central strategies to adapt billion-parameter foundation models while mitigating overfitting [19,10]. PEFT methods typically freeze the pre-trained model and adapt only a small set of parameters, making them highly relevant for medical domains with limited data and specialized institutional settings [4]. Representative directions include selective fine tuning [13], adapter based methods [14,23], and prompt based tuning [18,16].

A prominent PEFT approach is low-rank adaptation (LoRA) [15], which augments a frozen weight matrix  $W_0$  with a low-rank update  $\Delta W = BA$ , motivated by the hypothesis that task-specific updates lie in a low-dimensional subspace. Learning only these low-rank factors yields a favorable accuracy-efficiency trade-off relative to full fine-tuning. This mechanism has been extended to control parameter growth in continual medical image segmentation and personalized federated settings [5,21,4]. Despite its empirical success, standard LoRA has notable limitations. First, most low-rank adapters operate directly in feature space [28]. Moreover, in extreme resource-limited regimes—common in decentralized healthcare deployments—even conventional LoRA-style adapters can be non-trivial to store, distribute, and load, incurring storage and bandwidth overhead [12].

Recent works explore reparameterizing adaptation in a transformed domain to induce more structured updates. In the frequency domain, FouRA learns low-rank adaptations via Fourier projections [2], FourierFT explores compressing trainable updates via discrete Fourier parameterizations [12], and LoCA proposes selective frequency component learning [8]. These works suggest that frequency parameterizations can provide structured update spaces, which motivates wavelet-based alternatives that capture multi-scale structure. Wavelet transforms are widely used in deep learning as a principled tool for multi-scale representations. They have been integrated into scattering networks [3], transformer architectures [27], and generative modeling [20,11], demonstrating that multi-scale decompositions can improve both efficiency and fidelity.

In this work, we propose WaRA (Wavelet Low-Rank Adaptation), a PEFT approach for medical image classification that performs adaptation in a wavelet domain to exploit multi-scale structure. WaRA decomposes intermediate representations into frequency subbands that capture complementary information, performs low-rank updates in this transformed space, and reconstructs in the original domain. This wavelet-structured parameterization biases adaptation toward both coarse structure (low-frequency) and fine-grained features (high-frequency) that are prominent in medical imaging. We further develop Tiny-WaRA for extremely low-resource settings, which reduces the trainable budget by parameterizing the adapter update with a compact trainable core while keeping a fixed basis derived from pre-trained weights [1,22].

In summary, our key contributions are: (1) We present WaRA, a wavelet-domain low-rank adaptation module that leverages multi-scale subband decomposition to capture both global structure and fine-grained detail for medical image classification. (2) We develop Tiny-WaRA for extremely low-resource settings, substantially

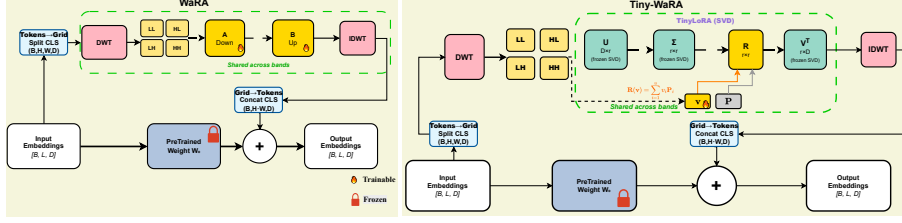


Fig. 1: **Overview of WaRA and Tiny-WaRA.** WaRA performs low-rank adaptation in a wavelet domain by applying DWT on patch tokens, updating subband coefficients with shared adapter parameters, and reconstructing an additive update via IDWT. Tiny-WaRA replaces the standard adapter with a compact parameterization that learns only a small coefficient vector in a fixed basis derived from pretrained weights [1,22].

reducing trainable parameters compared to baseline frequency-domain methods by learning a compact core update in a fixed basis derived from pre-trained weights. (3) We conduct extensive experiments on medical image classification benchmarks, complemented by targeted ablations and frequency-domain analyses that elucidate when and why wavelet-structured adaptation is effective.

## 2 Method

The core idea of WaRA, shown in Figure 1, is to perform parameter-efficient adaptation in a wavelet domain that exposes multi-scale structure while keeping the pretrained layer frozen. Consider a linear projection with frozen pretrained weights  $W_0 \in \mathbb{R}^{d_2 \times d_1}$  applied to token embeddings  $X \in \mathbb{R}^{B \times L \times d_1}$  ( $B$ : Batch Size,  $L$ : number of patch token + class token,  $d_1$ : Embedding size) which produces the base output  $Y_{\text{base}} = XW_0^\top$ . Standard LoRA adds an additive update using low-rank factors, that is  $\Delta W = BA$  with  $A \in \mathbb{R}^{r \times d_1}$  and  $B \in \mathbb{R}^{d_2 \times r}$  which  $r \ll d_1, d_2$  [15]. Inspired by LoRA, WaRA applies low-rank adaptation in the multi-scale wavelet domain rather than in the feature domain. Specifically, we split  $X$  into the class token  $X_{\text{cls}}$  and patch tokens  $X_{\text{tok}}$ , reshape the patch tokens into a spatial grid  $X_{\text{tok},r} \in \mathbb{R}^{B \times H \times W \times d_1}$ , and then apply a fixed 2D wavelet transform:

$$X = [X_{\text{cls}}, X_{\text{tok}}], \quad C = \mathcal{W}(X_{\text{tok},r}) = \{C_{\text{LL}}, C_{\text{LH}}, C_{\text{HL}}, C_{\text{HH}}\}, \quad (1)$$

where  $C_\alpha \in \mathbb{R}^{B \times H' \times W' \times d_1}$  and  $(H', W') = (H/2, W/2)$  for one level of decomposition, with  $\alpha$  indexing the wavelet subbands (e.g., LL, LH, HL, HH). In the wavelet domain, we apply a shared low-rank adapter along the feature dimension for every subband:

$$\Delta C_\alpha = C_\alpha A^\top B^\top, \quad A \in \mathbb{R}^{r \times d_1}, \quad B \in \mathbb{R}^{d_2 \times r}. \quad (2)$$

Parameter sharing across the four subbands avoids the parameter growth that would arise from using independent adapters per subband. We reconstruct the patch token update via the inverse transform, and we adapt the class token with the same adapter:

$$\Delta Y_{\text{tok}} = \mathcal{W}^{-1}(\{\Delta C_\alpha\}), \quad \Delta Y_{\text{cls}} = X_{\text{cls}} A^\top B^\top. \quad (3)$$

Finally, we form the layer output by residual fusion:

$$Y = Y_{\text{base}} + [\Delta Y_{\text{cls}}, \Delta Y_{\text{tok}}]. \quad (4)$$

### 2.1 Tiny-WaRA for extreme low resource adaptation

LoRA is efficient, but storing and training adapters can still be costly when many specializations are required or when the adaptation budget is extremely small. Tiny-WaRA reduces the trainable budget even more by parameterizing the adapter update with a compact trainable core on a fixed basis derived from  $W_0$  [1,22]. For each layer, we compute Singular Value Decomposition (SVD) and then truncate it to rank  $r$  by only keeping the  $r$ -largest singular values of pretrained weights:

$$W_0 \approx U \text{diag}(S) V^\top, \quad U \in \mathbb{R}^{d_2 \times r}, S \in \mathbb{R}^r, V \in \mathbb{R}^{d_1 \times r}. \quad (5)$$

We then define a mixing matrix as a linear combination of fixed basis matrices  $\{P_i\}_{i=1}^u$  (initialized with a Gaussian distribution) with a trainable coefficient vector  $v \in \mathbb{R}^u$  (with a zero initialization):

$$R(v) = \sum_{i=1}^u v_i P_i, \quad \Delta W(v) = U \text{diag}(S) R(v) V^\top, \quad (6)$$

so only  $v$  is trainable. Tiny-WaRA uses the same wavelet pipeline as WaRA, but replaces the subband update with  $\Delta W(v)$ :

$$\Delta C_\alpha = C_\alpha \Delta W(v)^\top, \quad \Delta Y_{\text{cls}} = X_{\text{cls}} \Delta W(v)^\top, \quad (7)$$

followed by IDWT reconstruction and residual fusion as above.

## 3 Results

### 3.1 Datasets, Training and Evaluation Setup

We evaluate on four medical image classification datasets, namely Messidor-2 [7], ISIC2018 [6], DDSM [17], and CXR COVID [24]. These correspond to 5-class diabetic retinopathy grading, 7-class skin lesion classification, 3-class mammography classification, and 3-class chest radiograph classification, respectively. For each dataset, we use the provided split directory with separate train, val, and test folders. We initialize the vision backbone with the BiomedCLIP ViT-B model

Table 1: Comparison results across four evaluation datasets. Per dataset columns report **F1** (%). ‘Params.’ denotes the ratio of learnable parameters to the total number of parameters. Entries are reported as mean±std. Among non gray rows, the best and second best means are colored blue and red, respectively

Method	Params.	Fundus (Messidor-2)	Dermoscopy (ISIC2018)	Mammography (DDSM)	Chest X-ray (COVID)	Avg. F1
Full fine tuning	100	39.04±5.01	67.46±1.17	72.19±0.71	97.50±0.40	69.05±1.82
Linear probing	0.0045	28.40±3.90	62.49±1.17	61.54±1.70	97.56±0.20	62.50±1.74
Bias	0.12	34.84±4.39	64.78±1.49	65.48±0.90	97.83±0.23	65.73±1.75
Prompt tuning [16]	0.176	30.58±3.88	62.94±1.02	62.38±2.35	97.36±0.26	63.31±1.88
Attention tuning [26]	33.04	30.42±8.18	63.26±2.23	62.88±1.21	97.31±0.56	63.47±3.05
Adapter [14]	2.05	25.68±9.67	67.22±2.12	65.97±2.61	<b>97.62±0.38</b>	64.12±3.69
LoRA (rank=16) [15]	0.69	39.69±3.07	<b>71.81±1.10</b>	68.22±7.04	96.40±0.84	69.03±3.01
LoRA (rank=8)	0.34	<b>40.50±4.55</b>	70.61±0.92	<b>73.96±1.77</b>	96.96±0.38	<b>70.51±1.90</b>
FourierFT [12]	0.16	18.63±1.03	39.90±1.18	62.24±1.91	92.44±0.95	53.30±1.27
LoCA [8]	0.17	31.36±2.44	58.11±2.02	62.65±1.22	95.93±0.38	62.01±1.52
FouRA [2]	0.68	37.60±4.63	71.30±1.22	67.47±4.20	<b>97.58±0.42</b>	68.49±1.66
WaRA (rank=8)	0.34	<b>45.35±2.60</b>	70.94±0.99	<b>74.68±0.94</b>	96.81±0.55	<b>71.94±1.27</b>
WaRA (rank=16)	0.69	38.73±7.07	<b>71.44±1.05</b>	70.20±2.61	96.64±0.26	69.25±2.75

using  $16 \times 16$  patches, and replace the classification head to match the dataset’s label space. All images are resized to  $224 \times 224$  and trained for 20 epochs with a batch size of 16. We use AdamW with weight decay 0.1 and a cosine learning rate schedule. We use a learning rate of  $2 \times 10^{-5}$  for full fine tuning,  $2 \times 10^{-4}$  for attention tuning, and  $2 \times 10^{-3}$  for the remaining parameter efficient methods, including WaRA. We select the best checkpoint using validation AUC and used a 16 GB NVIDIA V100 GPU to train all of our models. For all baselines, we follow the training configurations from their official repositories, and for FourierFT [12], LoCA [8], and FouRA [2], for matched parameter budget comparisons in Tiny-WaRA experiments (Table 3), we shrink their adaptation capacity to match the Tiny-WaRA parameter budget. Specifically, we reduce FourierFT by decreasing the number of learned Fourier components from 600 to 360, LoCA by lowering its low-rank adaptation size from 600 to 262, and FouRA by setting its rank to 64. For Tiny-WaRA, we use rank  $r = 64$  with basis size  $u = 128$ .

### 3.2 Comparisons with State-of-the-art

Tables 1 and 2 compare WaRA against representative parameter-efficient transfer learning baselines on four medical image classification datasets. Full fine-tuning provides a strong reference but updates all parameters, whereas linear probing is a low-cost lower bound and consistently underperforms. We report F1 scores in Table 1, where higher values indicate a better balance between sensitivity and precision at the operating threshold, a clinically relevant criterion that reflects improved decision-level performance and fewer false alarms.

According to Table 1, WaRA (rank=8) achieves the best overall performance among all methods, outperforming all parameter-efficient baselines. Compared to LoRA (rank=8), our strongest competitor, WaRA improves the average F1

Table 2: Average performance across the four datasets (%). Entries are reported as mean $\pm$ std, where the std term is the average of per dataset stds. Among non gray rows, the best and second best means are colored blue and red, respectively

Method	Params.	F1	ACC	AUC	Recall	Precision	Kappa
Full fine tuning	100	69.05 $\pm$ 1.82	78.12 $\pm$ 1.07	90.50 $\pm$ 0.42	67.75 $\pm$ 1.80	74.12 $\pm$ 4.00	73.43 $\pm$ 1.15
Linear probing	0.0045	62.50 $\pm$ 1.74	72.61 $\pm$ 2.72	86.71 $\pm$ 0.35	62.54 $\pm$ 2.02	66.77 $\pm$ 2.24	64.89 $\pm$ 2.89
Bias	0.12	65.73 $\pm$ 1.75	75.78 $\pm$ 0.86	88.76 $\pm$ 0.36	64.99 $\pm$ 2.05	68.99 $\pm$ 2.33	69.50 $\pm$ 2.63
Prompt tuning [16]	0.176	63.31 $\pm$ 1.88	74.34 $\pm$ 1.00	86.90 $\pm$ 0.28	62.45 $\pm$ 1.83	67.18 $\pm$ 2.36	66.68 $\pm$ 1.67
Attention tuning [26]	33.04	63.47 $\pm$ 3.05	73.54 $\pm$ 1.28	86.76 $\pm$ 1.08	63.23 $\pm$ 2.76	67.02 $\pm$ 4.89	66.13 $\pm$ 4.02
Adapter [14]	2.05	64.12 $\pm$ 3.69	75.47 $\pm$ 1.74	87.38 $\pm$ 2.10	63.57 $\pm$ 3.62	67.27 $\pm$ 4.58	64.35 $\pm$ 6.68
LoRA (rank=16)[15]	0.69	69.03 $\pm$ 3.01	76.91 $\pm$ 2.97	90.32 $\pm$ 1.14	68.27 $\pm$ 2.87	73.72 $\pm$ 3.15	73.03 $\pm$ 3.69
LoRA (rank=8)	0.34	<b>70.51<math>\pm</math>1.90</b>	<b>78.71<math>\pm</math>1.20</b>	<b>91.14<math>\pm</math>0.46</b>	<b>70.17<math>\pm</math>2.66</b>	<b>74.52<math>\pm</math>2.42</b>	<b>75.62<math>\pm</math>2.47</b>
FourierFT [12]	0.16	53.30 $\pm$ 1.27	71.69 $\pm$ 0.87	84.15 $\pm$ 1.49	53.08 $\pm$ 1.00	59.72 $\pm$ 3.36	53.98 $\pm$ 2.29
LoCA [8]	0.17	62.01 $\pm$ 1.52	74.26 $\pm$ 0.75	87.49 $\pm$ 0.26	60.98 $\pm$ 1.47	67.30 $\pm$ 1.73	64.43 $\pm$ 2.10
FouRA [2]	0.68	68.49 $\pm$ 1.66	77.28 $\pm$ 0.98	89.73 $\pm$ 0.85	67.57 $\pm$ 1.64	72.74 $\pm$ 1.76	72.39 $\pm$ 2.12
WaRA (rank=8)	0.34	<b>71.94<math>\pm</math>1.27</b>	<b>79.69<math>\pm</math>0.90</b>	<b>91.62<math>\pm</math>0.37</b>	<b>71.59<math>\pm</math>1.78</b>	<b>75.02<math>\pm</math>2.27</b>	<b>77.01<math>\pm</math>1.48</b>
WaRA (rank=16)	0.69	69.25 $\pm$ 2.75	77.22 $\pm$ 1.60	90.43 $\pm$ 0.79	69.05 $\pm$ 2.60	72.83 $\pm$ 3.58	72.81 $\pm$ 3.15

by +1.43 (71.94 vs. 70.51). The gains are most pronounced on Fundus (+4.85) and remain positive on Mammography (+0.72), while WaRA is slightly lower on Dermoscopy (-0.33) and comparable on Chest X-ray with a small difference (-0.81). We further report both ranks 8 and 16 for LoRA and WaRA; in both cases, rank=8 performs better overall, indicating that increasing the rank does not necessarily improve performance.

Additionally, Table 2 reports performance averaged across the four datasets over multiple metrics: F1 (harmonic mean of precision and recall), ACC (overall fraction of correct predictions), AUC (area under the ROC curve, measuring threshold-independent separability), Recall (true positive rate), Precision, and Cohen’s kappa (which measures agreement between predictions and ground truth while correcting for chance agreement, therefore generally more informative than accuracy under class imbalance). Consistent with Table 1, WaRA (rank=8) outperforms LoRA (rank=8) across all metrics in Table 2, while also exhibiting lower standard deviation, indicating more stable performance across runs.

We also compare against recent frequency-domain adaptation baselines, including FourierFT [12], LoCA [8], and FouRA [2]. FouRA is the strongest among these methods; nevertheless, WaRA (rank=8) improves over FouRA by substantial margins (e.g., +3.45 F1, +2.41 ACC, +1.89 AUC, +4.02 Recall, +2.28 Precision, and +4.62  $\kappa$ ). Overall, these results suggest that wavelet-based adaptation benefits from multi-resolution parameter updates that can capture both global structure and localized details more effectively than Fourier-based updates.

We next consider an ultra-low parameter regime in Table 3, where all methods are matched to a comparable trainable parameter budget by reducing their adaptation capacity. Tiny-WaRA trains a compact coefficient vector of size  $u = 128$  over a fixed basis while using rank  $r = 64$ , which yields only 0.0078% trainable parameters. Despite this severe constraint, Tiny-WaRA achieves an average AUC of 88.78 with 78.54 ACC and 69.43 F1, and it remains the top performer across the four datasets. This setting is practically important for

Table 3: Comparison results of Tiny-WaRA with selected PEFT baselines across four evaluation datasets. Per dataset columns report **AUC (%)**. ‘Params.’ denotes the ratio of learnable parameters to the total number of parameters. The best and second best results are bold and underlined, respectively.

Method	Computing cost Params.	Fundus (Messidor-2)	Dermoscopy (ISIC2018)	Mammography (DDSM)	Chest X-ray (COVID)	Performance (Avg.)		
						AUC	ACC	F1
FourierFT [12]	0.010	53.18	61.97	60.36	63.17	59.67	46.24	24.90
LoCA [8]	0.010	79.65	92.25	79.16	99.04	87.53	74.22	62.30
FouRA [2]	0.008	78.82	93.41	80.73	99.01	87.99	75.11	65.04
Tiny-WaRA (Ours)	0.0078	<b>81.05</b>	<b>93.48</b>	<b>81.47</b>	<b>99.22</b>	<b>88.78</b>	<b>78.54</b>	<b>69.43</b>

medical image classification as labeled data can be limited, and adaptation is often performed under tight memory, compute, and communication budgets, including on-premises deployment or privacy-preserving federated training, where the update size directly affects bandwidth and system cost [9].

### 3.3 Analysis and Ablation Study

**Wavelet energy across subbands.** Figure 2a reports the relative wavelet subband energy of the learned update across ViT layers on Fundus dataset. As shown, the LL band consistently carries the majority of the update energy, while the high frequency bands (LH, HL, HH) remain smaller but non-zero. This supports our design choice to fix and share the update parameterization across subbands, since allocating separate large capacity per band would be inefficient given the observed energy imbalance. At the same time, the presence of structured energy in the higher frequency bands, together with nontrivial CLS energy, indicates that the model still benefits from a fused multi resolution update, where coarse structure is primarily adjusted through LL and finer cues are injected through the remaining bands via the inverse wavelet reconstruction.

**Singular value spectrum of the update.** Figure 2b visualizes the singular value distributions of the effective weight updates ( $\Delta W$ ) generated by both LoRA and WaRA across all evaluated layers and datasets. In this plot, solid lines represent the mean spectra, while shaded areas indicate cross-layer and cross-dataset variance. Looking at the LoRA results (blue shaded regions), the singular values often drop rapidly. This steep decay implies that LoRA heavily biases its update capacity toward a small subset of dominant components. Although this intense focus can drive task specialization, it simultaneously makes the model more susceptible to overfitting and less robust to distribution shifts—a behavior consistent with existing literature describing LoRA updates as highly anisotropic [25]. WaRA, by contrast, yields a notably flatter spectrum with consistent variance, indicating that its update energy is dispersed much more evenly. This structural difference provides a compelling explanation for WaRA’s superior training stability and robustness: by preserving a richer array of update

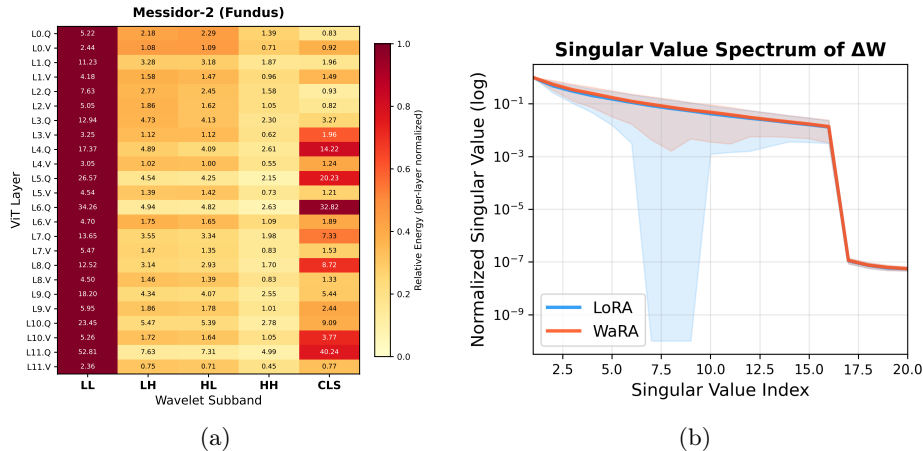


Fig. 2: Complementary analysis of WaRA. (a): Wavelet subband energy pattern on Fundus. (b): Singular value spectrum of the corresponding weight update.

Table 4: Ablation study on wavelet-subband adapter design (AUC, %).

Method	Messidor-2	ISIC2018	DDSM	COVID
WaRA (shared adapter across bands)	83.85	95.29	87.73	99.61
WaRA (band-specific adapters)	83.35	94.21	85.84	99.68

directions, WaRA avoids over-reliance on narrow features and generalizes more reliably across varied domains.

**Shared vs. band-specific adapters across wavelet subbands** In WaRA, we apply the same low-rank adapter parameters across all four wavelet subbands. A natural alternative is to assign independent LoRA adapters for different subbands, i.e., using separate  $(A_\alpha, B_\alpha)$  for each  $\alpha \in \{LL, LH, HL, HH\}$ , instead of sharing a single  $(A, B)$  across bands. Table 4 reports the ablation results. Sharing one adapter across subbands yields consistently better performance on Messidor-2, ISIC2018, and DDSM, while achieving comparable performance on COVID. Overall, the shared design improves the average AUC from 90.77 to 91.62 (+0.85), while also being more resource efficient due to the substantially reduced trainable footprint and optimizer overhead. These results support our design choice of subband sharing, indicating that the wavelet decomposition already provides complementary multi-resolution pathways, and allocating separate adapter capacity per band is unnecessary under the same training setup.

## 4 Conclusion

We introduced WaRA, a wavelet domain low-rank adaptation module for adapting BiomedCLIP ViT models to medical image classification. WaRA applies a fixed

wavelet decomposition to expose multi-resolution structure, then learns a shared low-rank update across subbands, therefore capturing both coarse context and fine details with a small trainable footprint. Across four modalities and datasets, WaRA consistently improves over strong parameter-efficient baselines, and Tiny-WaRA remains competitive in an extremely low parameter regime by learning a compact coefficient vector in a fixed SVD basis. Our analysis further supports the design, since the learned updates concentrate their energy in the LL band while still exploiting higher frequency cues, and WaRA exhibits a flatter singular value decay than LoRA, which indicates a less redundant update subspace.

## 5 Acknowledgments

This work was supported by the Canadian Foundation for Innovation-John R. Evans Leaders Fund (CFI-JELF) program grant number 42816. Mitacs Accelerate program grant number AWD024298-IT33280. We also acknowledge the support of the Natural Sciences and Engineering Research Council of Canada (NSERC), [RGPIN-2023-03575]. Cette recherche a été financée par le Conseil de recherches en sciences naturelles et en génie du Canada (CRSNG), [RGPIN-2023-03575].

## References

1. Bałazy, K., Banaei, M., Aberer, K., Tabor, J.: Lora-xs: Low-rank adaptation with extremely small number of parameters. arXiv preprint arXiv:2405.17604 (2024)
2. Borse, S., Kadambi, S., Pandey, N.P., Bhardwaj, K., Ganapathy, V., Priyadarshi, S., Garrepalli, R., Esteves, R., Hayat, M., Porikli, F.: Foura: Fourier low-rank adaptation. *Advances in Neural Information Processing Systems* **37**, 71504–71539 (2024)
3. Bruna, J., Mallat, S.: Invariant scattering convolution networks. *IEEE Transactions on Pattern Analysis and Machine Intelligence* **35**(8), 1872–1886 (2013)
4. Chen, J., Ma, B., Pan, Y., Pu, B., Cui, H., Xia, Y.: Personalized federated side-tuning for medical image classification. In: *International Conference on Medical Image Computing and Computer-Assisted Intervention*. pp. 452–462. Springer (2025)
5. Chen, Q., Zhu, L., He, H., Zhang, X., Zeng, S., Ren, Q., Lu, Y.: Low-rank mixture-of-experts for continual medical image segmentation. In: *International Conference on Medical Image Computing and Computer-Assisted Intervention*. pp. 382–392. Springer (2024)
6. Codella, N., Rotemberg, V., Tschandl, P., Celebi, M.E., Dusza, S., Gutman, D., Helba, B., Kalloo, A., Liopyris, K., Marchetti, M., et al.: Skin lesion analysis toward melanoma detection 2018: A challenge hosted by the international skin imaging collaboration (isic). arXiv preprint arXiv:1902.03368 (2019)
7. Decencière, E., Zhang, X., Cazuguel, G., Lay, B., Cochener, B., Trone, C., Gain, P., Ordóñez-Varela, J.R., Massin, P., Erginay, A., et al.: Feedback on a publicly distributed image database: the messidor database. *Image Analysis & Stereology* pp. 231–234 (2014)
8. Du, Z., Min, Y., Li, J., Lu, K., Zou, C., Peng, L., Chu, T., Gong, M.: Loca: Location-aware cosine adaptation for parameter-efficient fine-tuning. In: *The Thirteenth International Conference on Learning Representations*
9. Dutt, R., Ericsson, L., Sanchez, P., Tsaftaris, S.A., Hospedales, T.: Parameter-efficient fine-tuning for medical image analysis: The missed opportunity. arXiv preprint arXiv:2305.08252 (2023)
10. Fu, Z., Yang, H., So, A.M.C., Lam, W., Bing, L., Collier, N.: On the effectiveness of parameter-efficient fine-tuning. In: *Proceedings of the AAAI conference on artificial intelligence*. vol. 37, pp. 12799–12807 (2023)
11. Gao, S., Wang, R., Lu, C.: Contour wavelet diffusion for efficient and high-quality image synthesis. arXiv preprint arXiv:2305.10157 (2023)
12. Gao, Z., Wang, Q., Chen, A., Liu, Z., Wu, B., Chen, L., Li, J.: Parameter-efficient fine-tuning with discrete fourier transform. arXiv preprint arXiv:2405.03003 (2024)
13. Guo, D., Rush, A.M., Kim, Y.: Parameter-efficient transfer learning with diff pruning. arXiv preprint arXiv:2012.07463 (2020)
14. Houlby, N., Giurgiu, A., Jastrzebski, S., Morrone, B., De Laroussilhe, Q., Gesmundo, A., Attariyan, M., Gelly, S.: Parameter-efficient transfer learning for nlp. In: *International conference on machine learning*. pp. 2790–2799. PMLR (2019)
15. Hu, E.J., Shen, Y., Wallis, P., Allen-Zhu, Z., Li, Y., Wang, S., Wang, L., Chen, W., et al.: Lora: Low-rank adaptation of large language models. *ICLR* **1**(2), 3 (2022)
16. Jia, M., Tang, L., Chen, B.C., Cardie, C., Belongie, S., Hariharan, B., Lim, S.N.: Visual prompt tuning. In: *European conference on computer vision*. pp. 709–727. Springer (2022)

17. Lee, R.S., Gimenez, F., Hoogi, A., Miyake, K.K., Gorovoy, M., Rubin, D.L.: A curated mammography data set for use in computer-aided detection and diagnosis research. *Scientific data* **4**(1), 170177 (2017)
18. Lester, B., Al-Rfou, R., Constant, N.: The power of scale for parameter-efficient prompt tuning. arXiv preprint arXiv:2104.08691 (2021)
19. Li, W.H., Liu, X., Bilen, H.: Cross-domain few-shot learning with task-specific adapters. In: Proceedings of the IEEE/CVF conference on computer vision and pattern recognition. pp. 7161–7170 (2022)
20. Mattar, W., Levy, I., Sharon, N., Dekel, S.: Wavelets are all you need for autoregressive image generation. arXiv preprint arXiv:2406.19997 (2024)
21. Medghalchi, Y., Zakariaei, N., Rahmim, A., Hacıhaliloglu, I.: Synthetic vs. classic data augmentation: Impacts on breast ultrasound image classification. *IEEE Transactions on Ultrasonics, Ferroelectrics, and Frequency Control* (2025)
22. Morris, J.X., Mireshghallah, N., Ibrahim, M., Mahloujifar, S.: Learning to reason in 13 parameters. arXiv preprint arXiv:2602.04118 (2026)
23. Pfeiffer, J., Kamath, A., Rücklé, A., Cho, K., Gurevych, I.: Adapterfusion: Non-destructive task composition for transfer learning. arXiv preprint arXiv:2005.00247 (2020)
24. Siddhartha, M.: Covid cxr image dataset (research) (2021)
25. Song, Y., Zhao, J., Harris, I.G., Jyothi, S.A.: ShareLora: Parameter efficient and robust large language model fine-tuning via shared low-rank adaptation. arXiv preprint arXiv:2406.10785 (2024)
26. Touvron, H., Cord, M., El-Nouby, A., Verbeek, J., Jégou, H.: Three things everyone should know about vision transformers. In: European Conference on Computer Vision. pp. 497–515. Springer (2022)
27. Wang, H., Zhang, Y., Wang, L., Tian, Y.: Wavelet attention: Efficient wavelet-based transformer for visual tasks. arXiv preprint arXiv:2209.13789 (2022)
28. Zhang, Z., Sun, S., Wu, S., et al.: Parameter-efficient fine-tuning survey and benchmark. arXiv preprint arXiv:2303.15647 (2023)